Effect of illuminator partial coherence on optical tracking

Wilbur P. Brown * [a]
Directed Energy Directorate
Air Force Research Laboratory
Kirtland AFB, NM 87117

ABSTRACT

A technique for modeling the effect of illuminator partial coherence on target imaging and optical tracking is discussed. Computer simulations of imaging and tracking through atmospheric turbulence show that it is important to account for illuminator partial coherence if one is interested in accurately modeling the effects of turbulence on optical tracking.

Keywords: Imaging, tracking, turbulence, partial coherence

1. IMAGING WITH PARTIALLY COHERENT LIGHT

1.1 Background. The distinction between coherent, partially coherent and noncoherent imaging is, in part**, a function of the relative bandwidth of the illumination source and the bandwidth of the detector used to form the image. If the illumination is a single-line laser with a spectral width small compared to the detector bandwidth—and the object has a surface with roughness having scale lengths comparable to or greater than the laser wavelength—the image viewed from a fixed position has a speckle component superimposed on the unadulterated object irradiance. This speckle component/pattern is caused by the interference between random returns from surface irregularities within a region on the target comparable in extent to the Airy spot (as determined by the diffractive resolving power of the imaging system). This is an example of a coherent image. Nncoherent imaging occurs in the opposite limit where the detector bandwidth is vanishing small compared to the bandwidth of the illumination. Effectively, the detector averages over an infinite set of speckled image realizations by virtue of the disparity of the illumination and detector bandwidths. Partially coherent imaging occurs when the relative bandwidths of the illumination and detector are more nearly matched. The nature of the speckle patterns and the resulting summed image depends on the temporal coherence/bandwidth of the illumination light and the object depth.

For lack of a viable technique for modeling partially coherent imaging, it is commonly assumed that target imagery can be modeled as that obtained with noncoherent illumination—and that this can be achieved by adding a finite number of independent speckle realizations of the target image. There are at least two problems with this approach: 1) the target illumination is often provided by a finite bandwidth laser illuminator which is more like a partially coherent illuminator than an noncoherent illuminator; and 2) even if the illuminator were to approximate an noncoherent illuminator it is not clear how many independent speckle realizations are required to obtain a good approximation to the target image. Typically, the noncoherent image is approximated by the sum of a relatively few independent speckle realizations—the number of which is often dictated by computational run-time considerations rather than physics. In some cases this is acceptable. For example, it has been shown that in the modeling of the performance of a centroid tracker the use of relatively few speckle realizations yields reasonably accurate results. Typically, the 16 to 20 independent realizations provide sufficient accuracy. The problem is that centroid tracking does not work very well in scenarios where atmospheric turbulence causes significant amplitude scintillation. Thus, there is an interest in the modeling of more sophisticated tracking techniques which are inherently much more dependent on the exact nature of the target images. To model the performance of these techniques we need much more accurate target imagery.

Separate from the issue of target imaging, the nature of the illumination is also an important consideration in the modeling of the performance of adaptive optics systems which utilize one or more partially coherent illuminator beacons to create an extended reference source on the target. In directed

* email: wpbrown@linkline.com; phone: 818 887-2701

[a] current affiliation: consultant, MZA Associates Corporation

** Another factor is the source spatial coherence. A truly noncoherent source has a spatial coherence length equal to $\frac{\lambda}{\theta}$ where θ is the angular extent of the source. For example, the angular extent of the sun is approximately 0.5 degree and the lateral coherence length of solar radiation is of the order 60 μm in the visible. In contrast, the partially coherent laser illuminators of concern in this paper have essentially unlimited lateral coherence length; and, as a consequence, the spatial-temporal properties of the speckle patterns produced by such illuminators depend more significantly on target depth variations than those obtained with noncoherent illuminators.

energy applications where scintillation is an issue, the target is illuminated by two types of beacons. The discussion in the preceding paragraph concerned the imaging of a target illuminated by a one or more track beacons. The image obtained from the track beacons is used to steer the adaptive optics (AO) beacons onto a desired position on the target. These beacons are used as an adaptive optics reference source. The performance of the adaptive optics systems depends, in part, on the effective number of speckle realizations that the AO system detector integrates over; and thus, depends on the partial coherence properties of the illuminator and its interaction with the target depth profile. The techniques that we have developed for modeling partially coherent illuminators are directly applicable to both the target tracking and adaptive optics problems.

1.2 Partially Coherent Illuminator Model. We assume that the illuminators are lasers which support the oscillation of multiple longitudinal modes but no higher-order transverse modes. This implies that the laser output has finite temporal coherence but perfect spatial coherence. The longitudinal modes in a laser are equally spaced in frequency by c/2L where c is the velocity of light and L is the effective length of the laser resonator. The coherence length of the laser is determined by the number of longitudinal modes. The relation between the coherence length ℓ_c, the longitudinal mode spacing $c/2L$ and the number of modes N is

$$N \approx \frac{c/2\ell_c}{c/2L} = L/\ell_c \,.$$

Small coherence lengths are obtained with lasers which support oscillation over a very wide spectral passband. Examples of such lasers include the Ytterbium:yag laser—mode-locked versions of which are used to build picosecond and femtosecond pulsed lasers. A short coherence length illuminator differs only in that the longitudinal modes in such a laser are free-running rather than locked. The salient features of the output of such a laser are:

- On a time scale commensurate with the coherence time $\tau_c = \frac{\ell_c}{c}$, both the amplitude and phase of the laser output fluctuate
- The temporal variation of the laser output is periodic with period equal to the inverse of the longitudinal mode spacing $c/2L$.

In view of the fact that we have assumed that the illuminator laser output is spatially coherent, we can represent the illuminator field as the product of: 1.) a spatially invariant complex amplitude *pcs* which varies temporally at a rate determined by the laser coherence length; and 2.) a spatially and temporally varying component determined from the wave equation appropriate to propagation in turbulent media. The temporal variation of the second component occurs on a time scale set by the rate at which the atmosphere is changing and is much slower than that which occurs for the complex factor *pcs* accounting for the laser temporal bandwidth.

If we knew the shape of the laser gain spectrum we could compute the complex amplitude factor *pcs* as a sum of longitudinal mode contributions with amplitudes set by the gain spectrum. However, as we have no specific knowledge of the shape of the gain spectrum for the illuminator lasers of interest to us, we have adopted an adhoc model in which the complex amplitude factor is determined by the following requirements:

- The illuminator fringe visibility $\mathcal{V}$ is of the form

$$\begin{aligned} \mathcal{V} &= \exp[-\tau^2/2\tau_o^2] \,, \\ \tau_o &= \tau_c/2 \,. \end{aligned}$$

This requirement is satisfied for a random complex signal having the form

$$\begin{aligned} pcs(t) &= \int_{-\infty}^{\infty} d\omega \, [S(\omega)]^{1/2} a(\omega) \exp(i\omega t) \,, \\ S(\omega) &= \frac{1}{2\pi} \int_{-\infty}^{\infty} d\tau \mathcal{V}(\tau) \exp[-i\omega\tau] \,. \end{aligned}$$

where a is an uncorrelated random increment satisfying the relation (angular brackets denote a statistical average over an ensemble of realizations)

$$\begin{aligned} < d\omega_1 a(\omega_1) d\omega_2 a^*(\omega_2) > &= d\omega_1 \,, \quad \omega_1 = \omega_2 \\ &= 0 \,. \quad \omega_1 \neq \omega_2 \end{aligned}$$

• Regardless of the illuminator pulse length, the maximum number of independent speckle realizations resulting from the partially coherent illumination is limited to the number obtained in the period $2L/c$. For example, if the illuminator pulse is 30 ns long and the illumination laser resonator has length $L = 1$ m then the effective length of time over which the imaging detector integrates is $2L/c$ =6 ns rather than 30 ns.

1.3 Target Model. The target used in our studies is a canonical theater missile composed of a 3 m long, 0.88 m diameter cylinder capped with a 2.3 m cone at one end. The tip of the cone is rounded with a conformal sphere located 2.2 m from the junction of the cone and cylinder. The target surface is modeled as a Lambertian scatterer. In addition to the target reflectivity, the code computes target depth information which is used in the determination of the phase of the field reflected from the target.

1.4 Temporal Evolution of the Field Reflected From the Target. We assume that the target is illuminated by one or more beams propagated through turbulence. Multiple-beam illumination is used to mitigate the effect of illuminator scintillation at the target. We assume that the transmitter apertures of these beams are uniformly distributed around the periphery of the system pupil. The temporal coherence of the beams is specified in terms of a time delay which can be set to represent illuminators derived from the same laser or from independent lasers.

To obtain the field reflected from the target we sum the contribution from each of the illuminators. To account for effect of the finite temporal bandwidth of the illuminators, we recognize that the field of a finite bandwidth illuminator is equal to the product of the complex amplitude factor *pcs* associated with the temporal variation of the resonator output times the field that would be obtained with a single-line laser. The single-line laser field is calculated using the standard wave optics solution of the Helmholtz equation—as provided by our propagation code. The phase of the illuminator field at a plane z_o located slightly in front of the target is

$$\phi(x, y, z_o, t) = \phi_{atm}(x, y, z_o, t) + \phi_{src}(t)\,,$$
$$psc(t) = a_{src}(t)\exp[i\phi_{src}(t)]\,,$$

where ϕ_{atm} is a spatially and temporally varying phase due to the atmosphere and ϕ_{src} is a spatially invariant phase associated with the finite temporal bandwidth of the laser illuminator. The phase of the field reflected from the target and propagated back to the plane z_o is

$$\phi(x, y, z, t) = \phi_{atm}(x, y, z_o, t) + \phi_{src}(t - \frac{2z_s(x, y)}{c}) + \phi_{tgt}(x, y, z_s)\,.$$

z_s is the target surface depth and ϕ_{tgt} accounts for the phase shift contributed by target surface roughness. The reflected field at z_o is

$$u(x, y, z_o, t) = A\exp(i\phi)\,,$$
$$A = R_{tgt}(x, y)a_{src}(t - \frac{2z_s(x, y)}{c})a_{atm}(x, y, z_o, t)\,,$$

where R_{tgt} is the target reflectivity and a_{atm} is the contribution to the amplitude from the turbulence.

The temporal evolution of the field reflected from the target is caused by the interplay between the two-dimensional variation in target depth z_s and the temporal variation of the finite bandwidth laser signal. The importance of this temporal variation depends on the coherence length ℓ_c of the illuminator laser. If ℓ_c is sufficiently small relative to the target surface depth variation inherent in z_s, the temporal variability of the finite bandwidth illuminator results in a spatial-temporal variation in the phase and amplitude of the field reflected from the target—and this spatial-temporal variation results in a variation of the speckled target image on a time scale commensurate with the illuminator bandwidth. Likewise, if ℓ_c is sufficiently large relative to the surface depth variation inherent in z_s, the speckle pattern associated with the target image is relative invariant over the duration of the illuminator pulse.

1.5 Image Computation. The total field composed of the sum of the contributions from the individual illuminators is propagated to the imaging system pupil through the return path turbulence. The instantaneous image due to this field is then computed and added to the accumulated sum of images from previous time increments under the illuminator pulse. Effectively, two time scales are accounted for in the imaging simulation: a fast time scale which resolves the temporal variation under the illuminator pulse; and a slow time scale associated with the temporal development of the atmospheric turbulence. The fast time scale encompasses the times of the order of the laser coherence time ℓ_c/c, which may be as short as a few picoseconds, to times of the order of the illuminator pulse length which is typically a few tens of nanoseconds. On this time scale the atmosphere and target motion is effectively frozen. The

receiver responds to the average of the instantaneous speckle images produced by the temporal variation of the illuminator complex amplitude. The slow time scale is set primarily by target and receiver motion. Typically, this time scale is of the order of 1 ms or longer. On this time scale the target image changes relatively smoothly from one time increment to the next.

1.6 Computational Methodology. Although it is certainly possible to utilize a serial propagation code to model the partially coherent imaging process discussed here, it is far more practical to implement such a model using a parallel propagation code. We typically utilize 32 to 64 processors to do partially coherent imaging simulations. For example, consider the problem of simulating the imaging of a target illuminated with 8 lasers having an effective length of 1 m, a coherence length of 0.5 cm, and a pulse length of 30 ns. Assuming that the illuminator complex amplitude is sampled every τ_c seconds, the total number of illuminator time increments required to account for the number of time increments within the illuminator period is $2L/\ell_c = 400$. We could then proceed as follows:

- Use 32 processors
- Simultaneously propagate the 8 illuminator beams to the target through turbulence using 4 processors per illuminator
- Use 2 processors to propagate the field associated with 1 time increment within an illuminator pulse—which allows the propagation of 16 intra-pulse time increments in parallel using 32 processors. Do this 25 times to obtain 400 intra-pulse time increments per illuminator pulse.
- Sum the 400 intra-pulse images to obtain 1 frame of the image sequence seen by the detector.

1.7 Results. Undistorted imagery of the canonical target is shown in Figures 1–2. Figure 1 shows the near-field image of the target illuminated by a uniform illuminator beam incident at an angle of 30 degrees from normal incidence to the axis of rotation. The variation in the target irradiance is due to the Lambertian nature of the target reflectivity. Figure 2 shows the noncoherent target image formed by a diffraction-limited imaging system having a 1.5 m pupil located 270 km from the target. The smoothing seen in this image is caused by the finite resolving power of the imaging system.

Figure 3 shows a sequence of images obtained by adding independent coherent speckle images of the target. The path between the target and the imaging system is vacuum so that atmospheric distortions associated with turbulence are not present in these images. In the limit of a very large number of speckle realization one expects this image to be the noncoherent image observed in vacuum. It is interesting to note that even after summing several thousand independent speckle images the speckle-averaged image shows discernible differences from the noncoherent image. The importance of these differences depends on the application. We have found, for example, that centroid tracking is relatively insensitive to the fine details in the noncoherent image and therefore relatively few speckle realizations are needed to model centroid tracker performance. However, other tracking techniques which utilize more detailed target information—e.g., edge tracking algorithms—typically require higher-fidelity imagery and therefore more speckle realizations to model noncoherent target imagery.

Figure 4 shows a sequence of images obtained within/under a partially coherent illuminator pulse. The partially coherent illuminator used in this case is spatially uniform with a finite bandwidth such that the coherence length is 0.5 cm. The path between the target and the imaging system is vacuum. The effective length of the illuminator resonator is assumed to be long enough that the period of the illuminator field significantly exceeds the pulse length—which is admittedly not very practical because this requires that the the effective resonator length significantly exceed $1600\ell_c$ =8 m. But we have done this to examine the evolution of the partially coherent image over a number of coherence times comparable to the number of independent speckle realizations used to obtain the speckle-averaged imaging results shown in Figure 3. Note that the speckle averaging which occurs under the partially coherent illuminator pulse is incomplete even after 3200 coherence times. We believe that this is due to the fact that the 0.5 cm coherence length of the incident illumination is not sufficiently small relative to the target depth variation to effectively average the coherent return from the target. This is especially true for reflections originating from the region in the vicinity of the axis of symmetry where the target depth varies most slowly. Typically, the illuminator laser resonator would have an effective length of the order 1 m. In this case, the partially coherent image in vacuum would correspond to the image on the left side of the middle row of images in Figure 4, which is obtained by integrating over 320 coherence times.

Figure 5 shows a sequence of images obtained by adding independent coherent speckle images of the target for a case in which the atmosphere is turbulent. The target illumination was provided by a multi-beam illuminator (8 beams) propagated from the transmitter to the target through turbulence. It is interesting to note that qualitatively the distorted target image appears to converge to a stable, unchanging, image more quickly in this case than it did in vacuum (see Figure 3). In each case, however, the level of fluctuation in the image decreases steadily with the number of images contained in the average. The image obtained by averaging 3200 independent coherent speckle images is probably a very

good approximation to that which would be obtained from an noncoherent illuminator. Likewise, the speckle-averaged image obtained from the sum of 320 independent coherent speckle images—shown on the left side of the second row of images in Figure 5—approximates the image that would be obtained with partially coherent illumination from a resonator having an effective length of the order of 1 m.

Figure 6 shows a sequence of images obtained within/under a partially coherent illuminator pulse for a case in which the atmosphere is turbulent (not the same atmosphere used to generate the images in Figure 5). The target illumination was provided by a multi-beam illuminator (8 beams) propagated from the transmitter to the target through turbulence. The 8 illuminator beams were statistically independent and each had a coherence length of 0.5 cm. The target images shown in Figure 6 are obtained from a cumulative sum of the images obtained at the 1st, 16th, 100th and 200th time increment where the time increment was equal to the coherence time. The most highly scintillated image is obtained at the 1st time increment and is effectively a single coherent speckle realization. The image obtained from the cumulative sum of the first 16 time increment is qualitatively similar to the image on the left side of the top row of images in Figure 5—which is to be expected since both images are obtained by summing 16 coherent speckle realizations. Likewise, it is apparent that the partially coherent images obtained from the sum of 100 and 200 time increments are converging to a stable result.

Figure 7 shows the temporal development of a partially coherent image on a time scale commensurate with the rate at which the atmosphere changes. The time increment in this case is the interpulse period which is assumed to be 0.1 ms (as opposed to the coherence time of the partially coherent illuminator τ_c which is 16.7 ps if the coherence length is 0.5 cm). The top row of images in Figure 7 shows the partially coherent images obtained for the 1st and 2nd illuminator pulses. The bottom row of images shows the partially coherent images obtained for the 10th and 11th pulses. The thing to note about these images is that on a 0.1 ms timescale the character of the image changes smoothly from pulse to pulse. This differs from the behavior observed when the speckle averaging method is used to simulate the target imagery and relatively few speckle realizations are used to form this image. For example, for the case where the speckle-averaged image is obtained from 16 speckle realizations the images obtained from successive pulses are essentially uncorrelated.[1] As expected, substantial changes in the character of the images occur on a time scale equal to 10 interpulse periods.

2. COMPARISON OF TRACKING RESULTS

2.1 Background. We have applied the leading-edge tracking algorithm described in Section 2.5 to target imagery computed in three ways: 1) a sum of independent speckle realizations; 2) an approximation to noncoherent imagery based on the summation of returns from a closely-spaced array of point sources on the target—which we refer to as the point spread function (PSF) model; and 3) the summation of images under a set of partially coherent illuminator pulses. The purpose of this study was to determine the sensitivity of the tracking results to the type of imaging model used in the simulation. Moreover, we wanted to determine the best approach to the target modeling given the constraint that the computational effort be approximately the same whatever the approach used to model the imagery. To do this comparison, we assumed that a partially coherent image formed by the sum of 416 time increments under a partially coherent illumination pulse is an appropriate standard to compare to—i.e., this image is for all practical purposes that which will occur under conditions of interest. We arrived at this based on the assumption that the illuminator lasers have a coherence length of 0.5 cm, a resonator length of 1 meter and a pulse length greater than the period of the laser output (period=2L/c=6.67 ns).*

2.2 Implementation of the Speckle-Averaged Imaging Model. In the speckle-averaged imaging model the target image is computed by summing the speckle images obtained for a set of target fields of the form

$$u_s(\mathbf{x}) = A(\mathbf{x}) \exp[i\phi_s(\mathbf{x})] \,, \quad s = 1, 2, 3, ..., N$$

where A is computed from the illuminator fields as the square root of the sum of the illuminator irradiances times the target reflectivity and the phase distributions ϕ_s are independent samples of random realizations of target phase. It should be noted that this model does not accurately represent the effect of multiple beam illumination. For example, with 4 beam illumination the speckle image seen by a detector for a particular random phase realization ϕ_s is the sum of four speckle images—one for each of the illuminators. In contrast, we have represented the effect of the multiple illumination beams by adding irradiances to obtain an effective illumination amplitude (i.e., the amplitude A). We have done

* In our simulation the time increment under the pulse was equal to the coherence time ℓ_c/c. Thus, the total number of time increments contained within a time equal to the period of the laser output is $\frac{2L/c}{\ell_c/c} = 2L/\ell_c = 400$. We computed 416 time increments to allow us added flexibility in choosing the number of time increments to propagate in parallel.

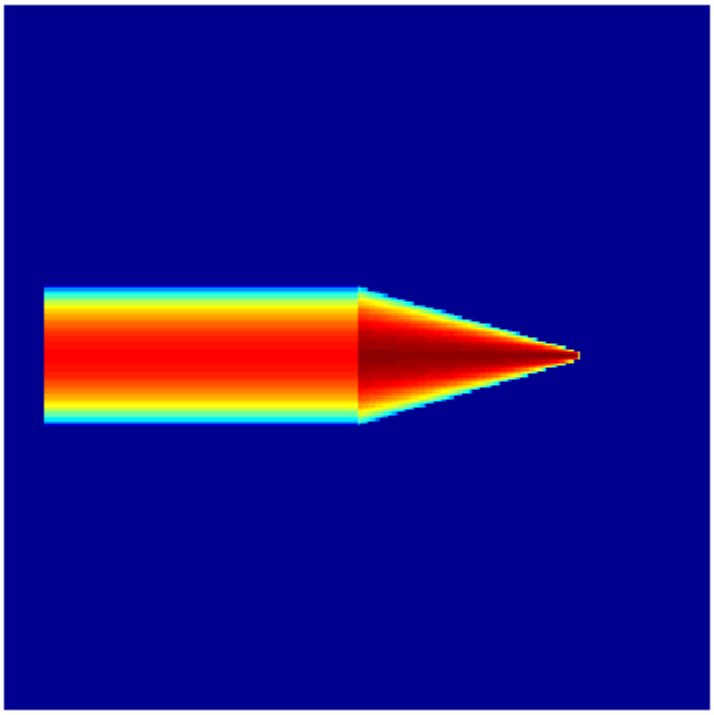

Figure 1. Canonical target uniformly illuminated at an angle 30 degrees to the cylinder axis.

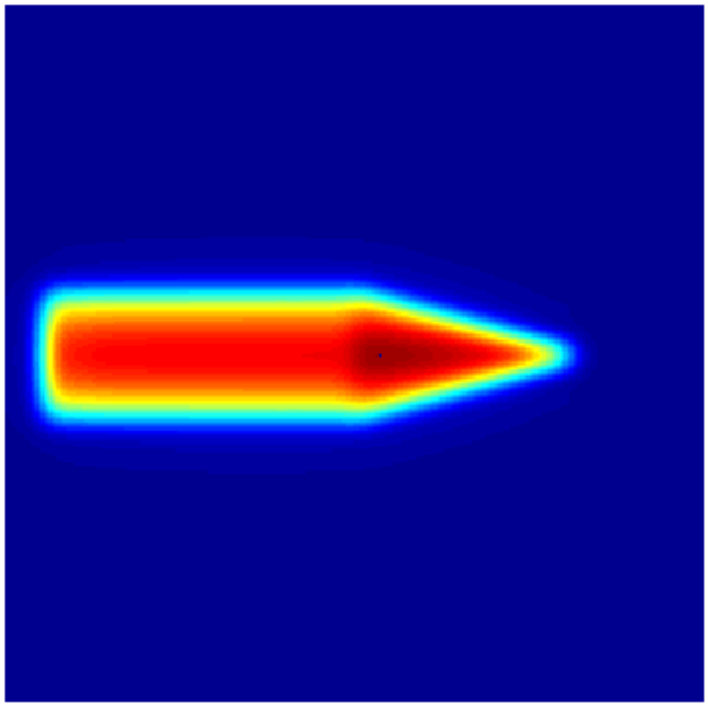

Figure 2. Noncoherent image of canonical target uniformly illuminated at an angle 30 degrees to the cylinder axis.

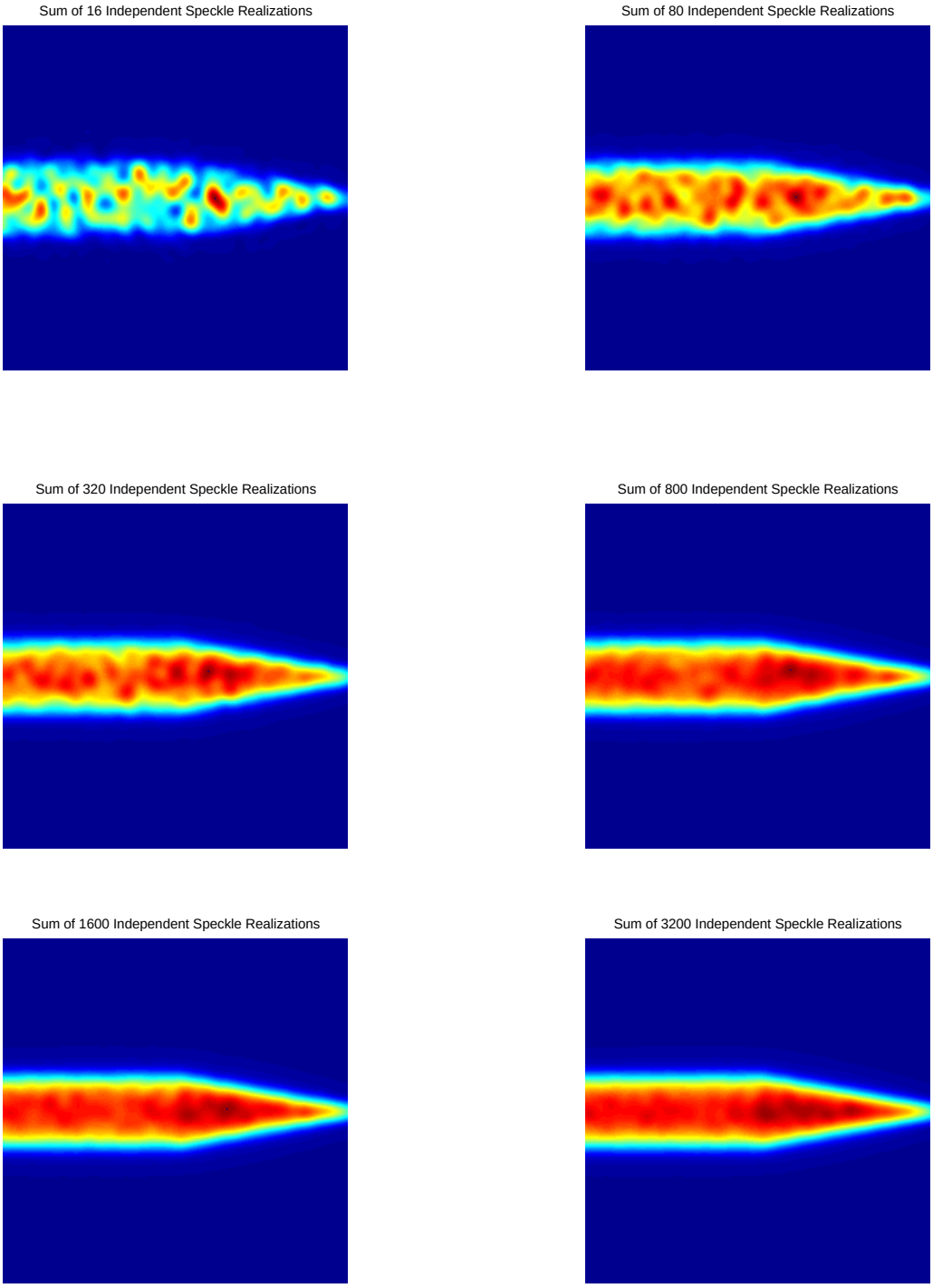

Figure 3. Speckle-averaged imaging of a uniformly illuminated target in vacuum.

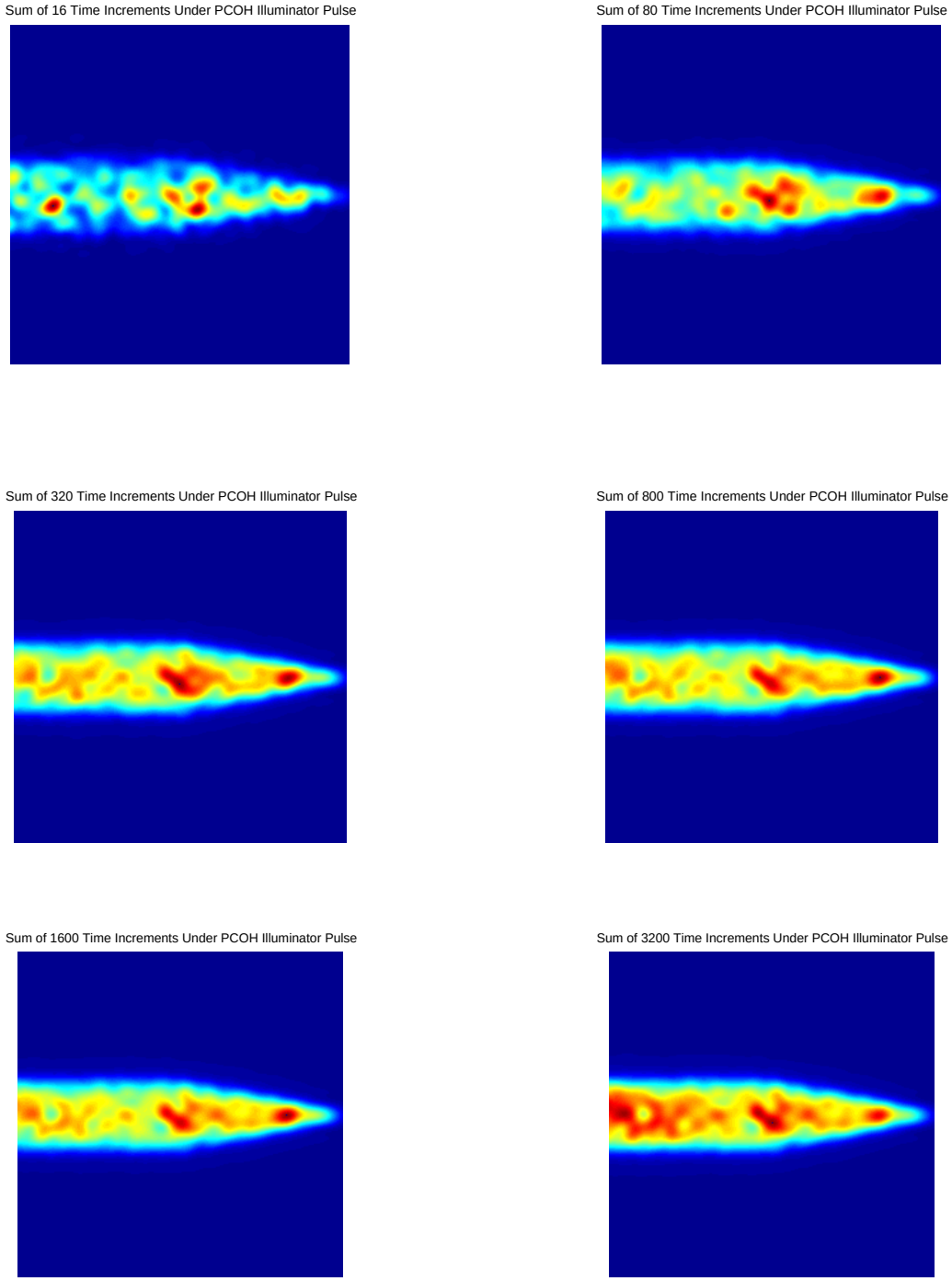

Figure 4. Partially coherent imaging of a uniformly illuminated target in vacuum within the illuminator pulse.

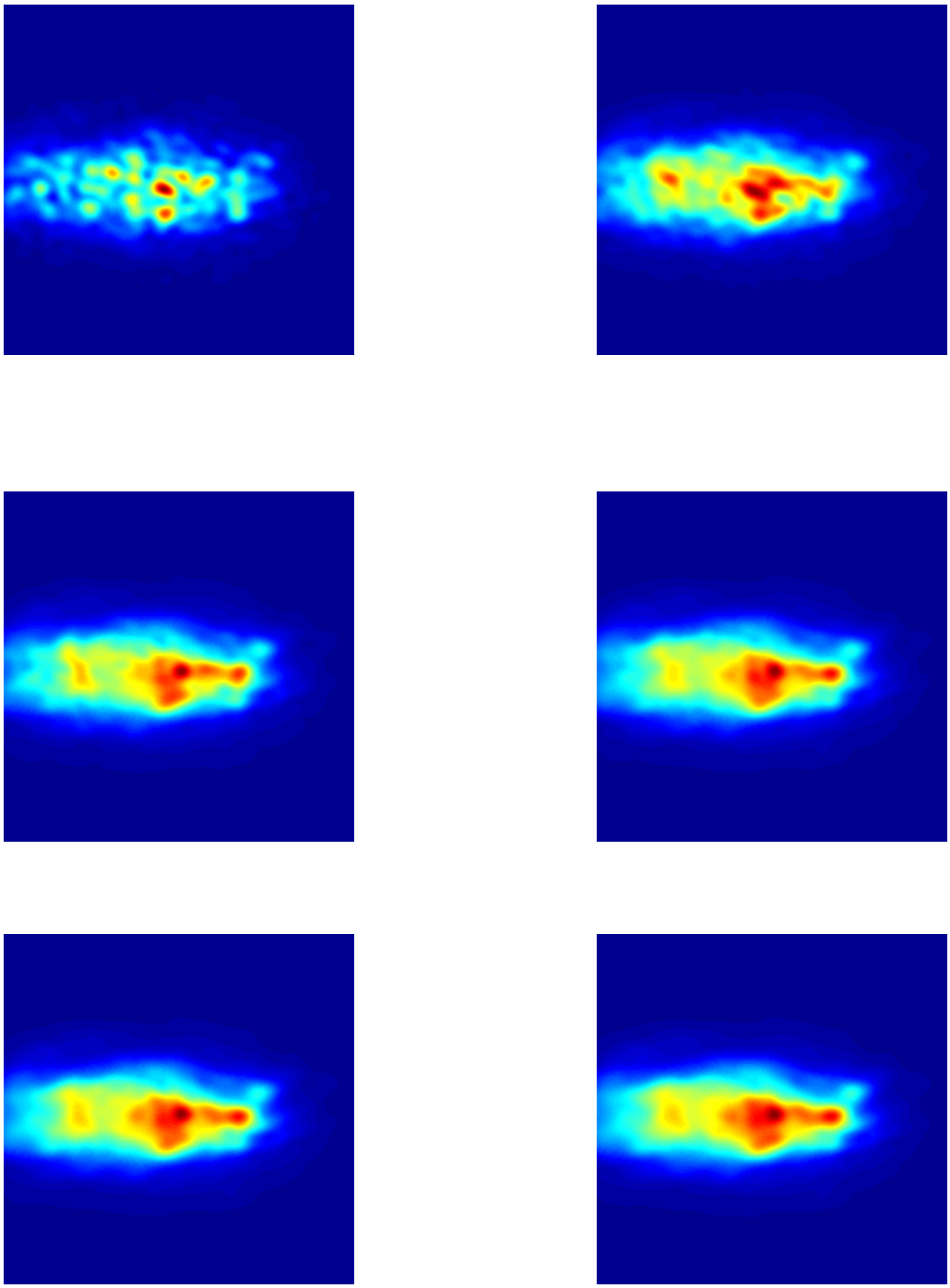

Figure 5. Speckle-averaged imaging. The top left and right images, the middle left and right images, and the bottom left and right images were obtained from the average of 16, 80, 320, 800, 1600 and 3200 independent speckle realizations.

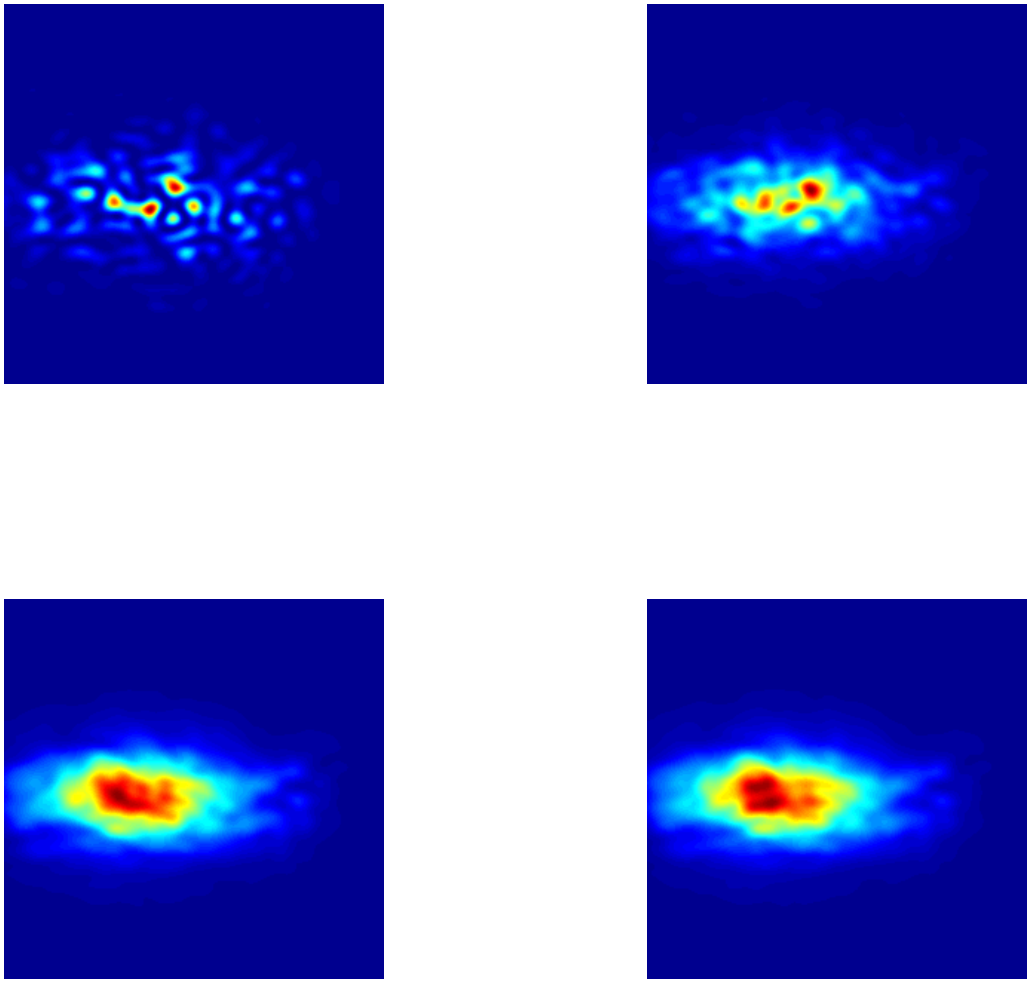

Figure 6. Imagery within a partially coherent illuminator pulse. The upper left, upper right, bottom left and bottom right images are those obtained at the 1st, 16th, 100th and 200th time increment where a time increment is equal to the illuminator coherence time.

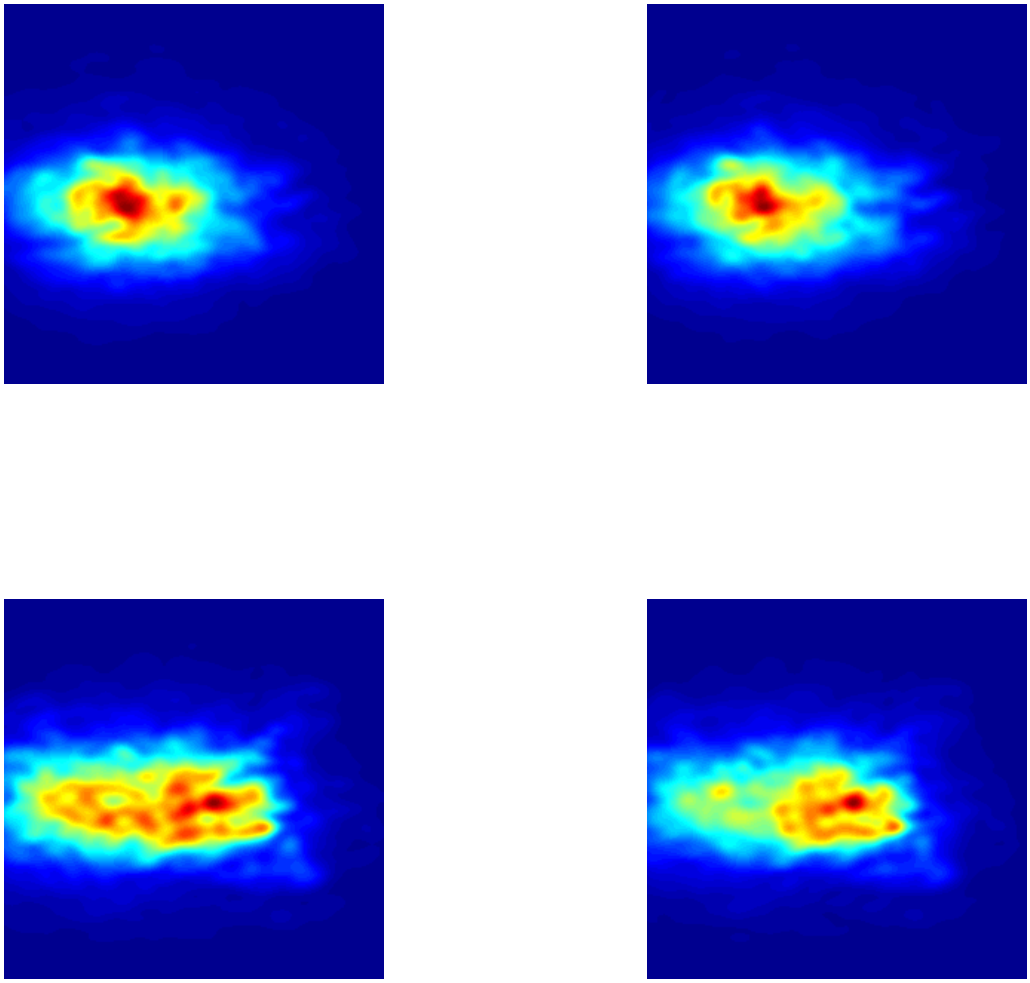

Figure 7. Temporal development of target image. The image on the upper left is that obtained by averaging over the first partially coherent illuminator pulse. The images on the upper right, lower left and lower right are those obtained from the second, tenth and eleventh illuminator pulses.

Figure 8. Diffraction-limited image of PSF target model in vacuum

this because this is the way that most codes implement speckle-averaged imaging. This reduces the computational burden by a factor equal to the number of illuminators—at the expense of failing to accurately represent the effect of multiple beam illumination on the speckle averaging process.

2.3 Implementation of the Point Spread Function (PSF) Model. In the PSF model the target image is approximated by the image obtained by summing the images from an array of point sources located on the target. The results discussed in this paper were obtained from an array of 288 Gaussian beam "point sources" having a field of the form

$$u_j(\mathbf{x}) = A(\mathbf{x}) exp\big[-\frac{|\mathbf{x}-\mathbf{x}_j|^2}{2\rho_o^2}\big]\,,$$
$$\rho_o = d/3\,,$$

where $\mathbf{x}_j$ is the location of the source, and d is the diameter of a circle containing approximately 90 percent of the energy. We refer to d as the "diameter" of the point source. The point sources were distributed on the target with 136 used to cover the cone and 152 on the cylindrical body. The point

sources on the cone were arranged in a triangular configuration with a base to height ratio of 0.4 .* The remaining 152 points were arranged in a rectangular configuration, again with a base to height ratio of 0.4 . Approximately 1.37 meters of the target cylinder (body) is covered by the 152 point sources used on the body, whereas the target cone is completely covered by the 136 point sources used on the cone. The diameter of the point sources is 7cm for the results presented here.

As in the case of the speckle-averaged image model, the amplitude A of the point source fields is set to the square root of the product of the sum of the illuminator irradiances times the target reflectivity. The use of the amplitude A defined in this way doesn't suffer the same limitations mentioned above in regard to the speckle-averaged imaging model because the PSF model applies to the case where the imaging is truly noncoherent and speckle averaging is not an issue—i.e., it is assumed that the number of speckle realizations is essentially infinite, in which case we don't have to worry about accurately representing the effect of the multiple beam illumination other than its effect on the net illumination of the target.

2.4 Qualitative Comparison of Target Imagery Obtained With the Three Methods. The PSF model diffraction-limited image of the target computed for vacuum propagation is shown in Figure 8. In this case the target is uniformly illuminated. This image is essentially the same as the ideal diffraction-limited noncoherent image with the exception that we have not completely populated the target body/cylinder with point sources. In addition, it differs from the diffraction-limited image shown in Figure 2 in that the cone is 2.3 meters long instead of the 1.5 meter cone shown in Figure 2. In fact, all of the images shown in this paper are for a target with a 2.3 meter cone, with the exception of those shown in Figures 1 and 2. The computational parameters used to obtain this image and those in Figures 9–17 are: computational mesh size 1024x1024; turbulence phase screen size 1024x2048; computational mesh spacing 1.75 cm; turbulence outer scale length 10 meters; turbulence inner scale length 1 cm**; Clear 1 night turbulence model.[2]

The images in Figures 9–11 apply to a turbulence realization where the strength was 0.5 times that of the Clear 1 profile; those in Figures 12–14 to the same turbulence realization but with a strength equal to 1.0 times the Clear 1 model; and those in Figures 15–17 to the same turbulence realization but with a strength equal to 2.0 times the Clear 1 model. As indicated above, the partially coherent images are obtained by summing 416 instantaneous speckle images under the partially coherent illuminator pulse. The speckle-averaged images in Figures 10, 13, and 16 were obtained by summing 416 independent speckle images. Likewise, as indicated above, the PSF image is obtained by summing the images of 288 point sources uniformly distributed over the target body.

For a given strength of turbulence, the images obtained with the three different methods are qualitatively similar with regard to their gross features. With regard to the fine detail in the images it appears that the images become progressively smoother as one goes from the partially coherent to the speckle-averaged to the PSF images. Theoretically the speckled-averaged image should look like the PSF image as the number of independent speckle realizations is increased—but we have seen that this requires a very large number of speckle realizations (e.g., see Figure 3). In weak turbulence the speckle-averaged and PSF images are strikingly similar. This is less so in the stronger turbulence but it is clear that the speckle-averaged image is more like the PSF image than the partially coherent image regardless of the of the strength of the turbulence.

2.5 Leading-Edge Track Algorithm. The algorithm we used identifies a set of points to be used in the calculation of a target centroid. In this algorithm the points used are the first 19 pixels with irradiance above a threshold level set by the product of an adhoc threshold factor and the irradiance of the pixel having the maximum value. In most of the calculations we used a threshold factor equal to 0.05. In doing the search for candidate pixels we assume that the direction of the target trajectory is known. The search is carried out along successive columns of pixels aligned perpendicular to the direction of motion—starting with the most forward column of pixels. The location of the centroid determined by this calculation depends on the threshold factor. Lowering the threshold moves the centroid toward the target leading edge and raising it moves it further away from the leading edge.

In applying this algorithm to the simulated target imagery, we have used a reduced resolution image that accounts for the finite size of the track camera pixels. Somewhat arbitrarily we have assumed that the track camera pixel covers 16 simulation pixels. The pixel in the full resolution simulated image has

* This configuration was chosen such that the base to height ratio was equal to the that of the cone—which guarantees that the point sources are evenly distributed over the surface of the cone (i.e., evenly distributed on the flat projection of the surface on a plane through the axis of symmetry of the cone.)

** Inner scale behavior represented by the spectral cutoff model developed by Reginald Hill, as approximated by J. H. Churnside[3]

pcoh_image_416_ipix=16_xclr1=.5_npulse=50_lambda=1.03_dynamic_md_tgt_image.ps

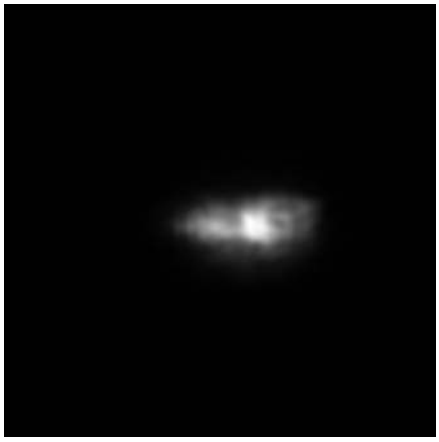

Figure 9. Partially coherent image of a target illuminated by four beams in turbulence having a strength equal to 0.5 times the Clear 1 value.

spckl_image_416_ipix=16_xclr1=.5_npulse=50_lambda=1.03_dynamic_md_tgt_image.ps

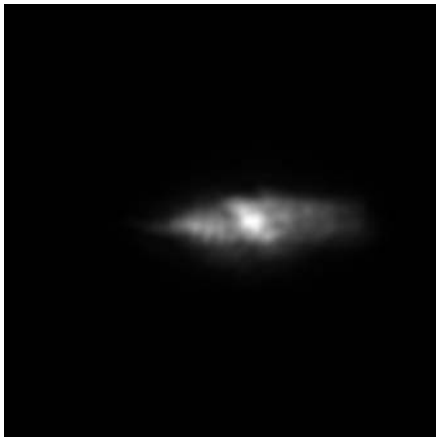

Figure 10. Speckle-averaged image of a target illuminated by four beams in turbulence having a strength equal to 0.5 times the Clear 1 value.

psf_image_md_nref_tot=288_ipix=16_xclr1=.5_npulse=1_tgt_image.ps

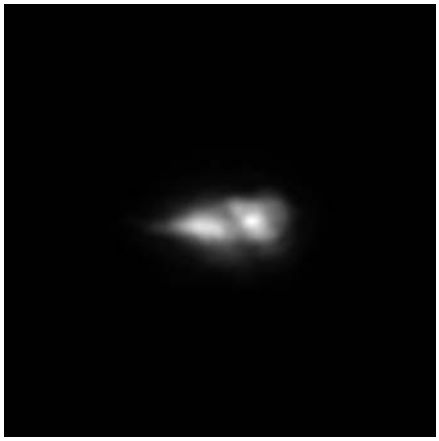

Figure 11. PSF image of a target illuminated by four beams in turbulence having a strength equal to 0.5 times the Clear 1 value

pcoh_image_416_ipix=16_xclr1=1_npulse=50_lambda=1.03_dynamic_md_tgt_image.ps

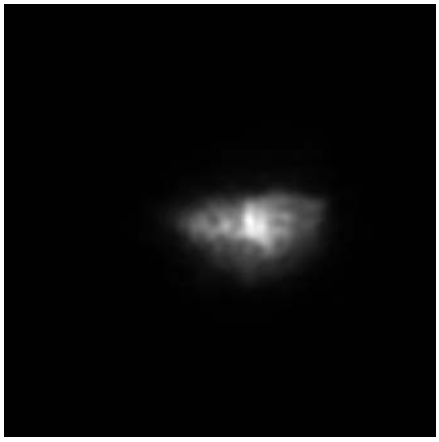

Figure 12. Partially coherent image of a target illuminated by four beams in turbulence having a strength equal to 1.0 times the Clear 1 value.

spckl_image_416_ipix=16_xclr1=1_npulse=50_lambda=1.03_dynamic_md_tgt_image.ps

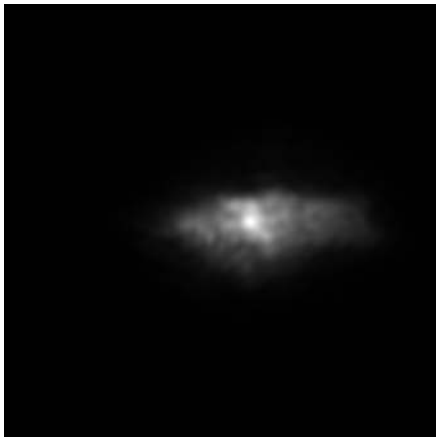

Figure 13. Speckle-averaged image of a target illuminated by four beams in turbulence having a strength equal to 1.0 times the Clear 1 value.

psf_image_md_nref_tot=288_ipix=16_xclr1=1_npulse=1_tgt_image.ps

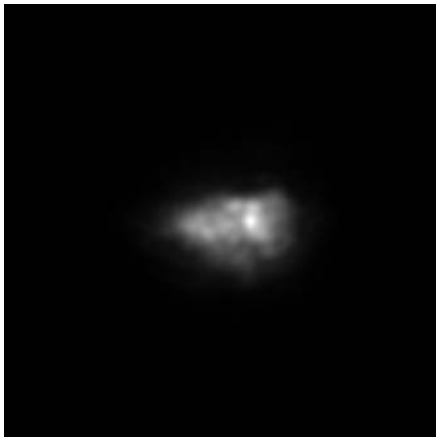

Figure 14. PSF image of a target illuminated by four beams in turbulence having a strength equal to 1.0 times the Clear 1 value

pcoh_image_416_ipix=16_xclr1=2_npulse=50_lambda=1.03_dynamic_md_tgt_image.ps

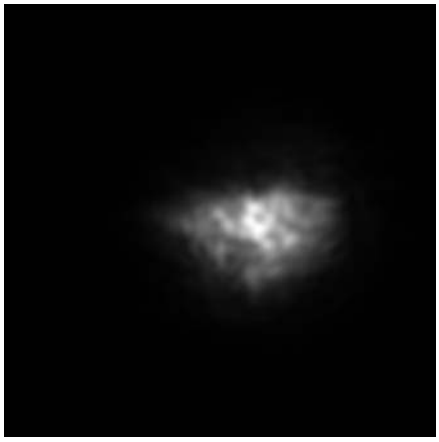

Figure 15. Partially coherent image of a target illuminated by four beams in turbulence having a strength equal to 2.0 times the Clear 1 value.

spckl_image_416_ipix=16_xclr1=2_npulse=50_lambda=1.03_dynamic_md_tgt_image.ps

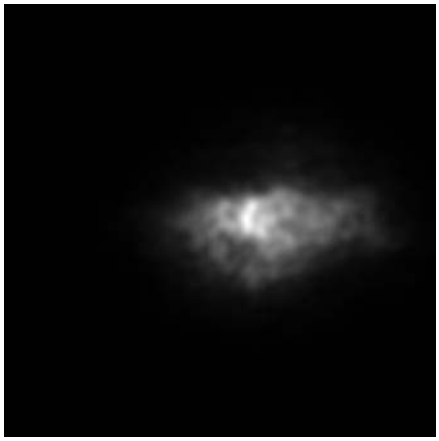

Figure 16. Speckle-averaged image of a target illuminated by four beams in turbulence having a strength equal to 2.0 times the Clear 1 value.

psf_image_md_nref_tot=288_ipix=16_xclr1=2_npulse=64_tgt_image.ps

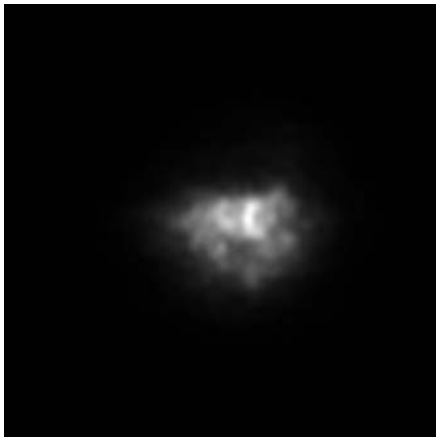

Figure 17. PSF image of a target illuminated by four beams in turbulence having a strength equal to 2.0 times the Clear 1 value.

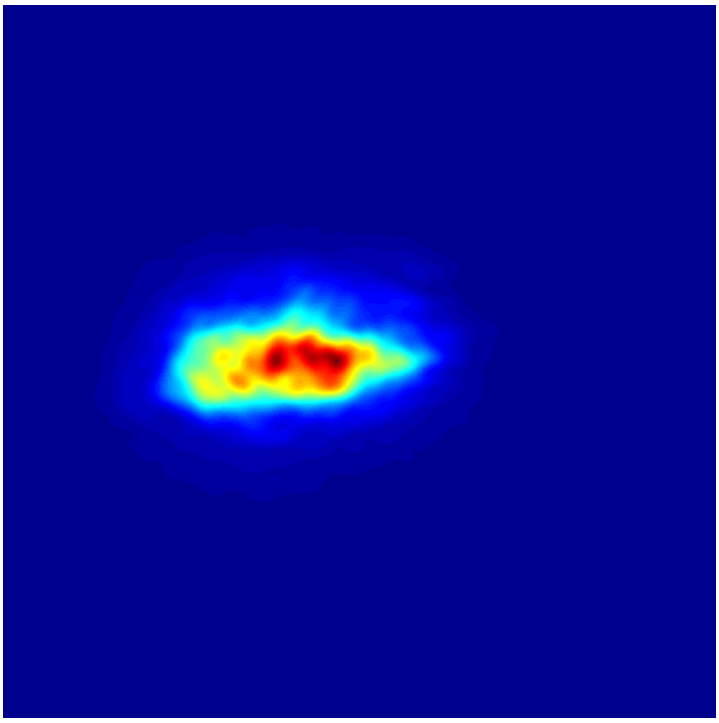

Figure 18. Full resolution target image—0.057 μrad pixels

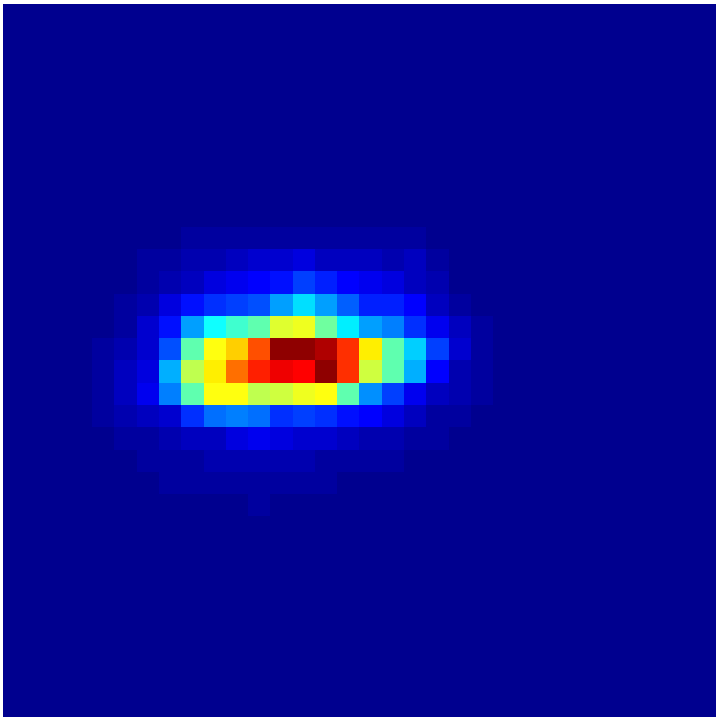

Figure 19. Reduced resolution target image—0.92 μrad pixels

an angular extent $\delta\theta$ given by the relation

$$\delta\theta = \frac{\lambda}{Ndx}$$

where λ (1.03μm) is the illuminator wavelength, N is the computational mesh size (1024), and dx is the mesh spacing (1.75 cm). Figures 18 and 19 show a partially coherent target image before and after the re-pixelization.

Comparison of Computed Target Jitter. Sample results for target jitter along two orthogonal axes are shown in Figures 20–21. Figure 20 shows results for the jitter along the axis of symmetry of the target. We refer to this component of the jitter as the longitudinal jitter. Figure 21 shows results for the jitter along a direction perpendicular to the axes of symmetry. This jitter is referred to as the transverse jitter. In these figures the notation used in labeling the PCOH and SPCKL results—e.g., pcoh26 and spckl26—indicates that they apply to target images obtained by averaging over 26x16=416 partially coherent time increments under a partially coherent pulse or over 26x16=416 independent speckle realizations in the case of SPCKL imaging. This notation is used because in some cases we used a smaller number of images in the averaging process—but always did this modulo 16—which is the number of images computed in parallel by the code. Thus, the notation pcoh1, spckl1 would refer to images computed from the sum of 16 time increments under a partially coherent pulse or from the addition of 16 independent speckle images.

There are three things to be noted from the results in Figures 20 and 21: 1) as expected, the longitudinal jitter is substantially larger than the transverse jitter; 2) in the case of the transverse jitter the three imaging techniques give results that agree relatively well; and 3) in the case of the longitudinal jitter the SPCKL and PSF results agree relatively well, whereas the PCOH results differ noticeably from those obtained with the other two methods. Based on our argument that the imaging of laser-illuminated targets is most likely to be of the partially coherent type, these results suggest that it would be best to use a partially coherent imaging simulation in modeling the tracking of such targets. As indicated above, these results apply to a case where we used 416 partially coherent time increments and 416 independent speckle images to form the target images—which is not practical to do for detailed modeling of tracking systems. Thus, we also compared results obtained when the number of image sequences was less than 26. The result of these calculations is that we found that the partially coherent imaging simulation had the lowest error relative to a full blown 416 image simulation regardless of the number of 16 images sequences used to form the target image—i.e., for a given amount of computational effort the reduced partially coherent image simulation provided the best approximation to what we believe is truth.

ACKNOWLEDGMENTS

This work was performed mainly while the author was an IPA with the Directed Energy Directorate of the Air Force Research Laboratory (AFRL/DE) at Kirtland AFB NM. More recently the work has continued under a consulting agreement with AFRL/DE contractor MZA Associates Corporation. The computer simulations were performed at the Maui High Performance Computing Center. Computer allocations were provided by the DOD Challenge Program managed by the High Performance Computing Modernization Office.

REFERENCES

1 P. H. Merritt, private communication.

2 R. R. Beland,"Propagation through atmospheric optical turbulence," Chap 2, Vol 2, **The Infrared and Electro-Optical Systems Handbook**, F. G. Smith editor, 3rd Edn. , ERIM/SPIE Press, Bellingham, WA, 1993.

3 J. H. Churnside,"A spectrum of refractive index in the turbulent atmosphere," *J. Modern Opt.* **37**, 13–16, 1990.

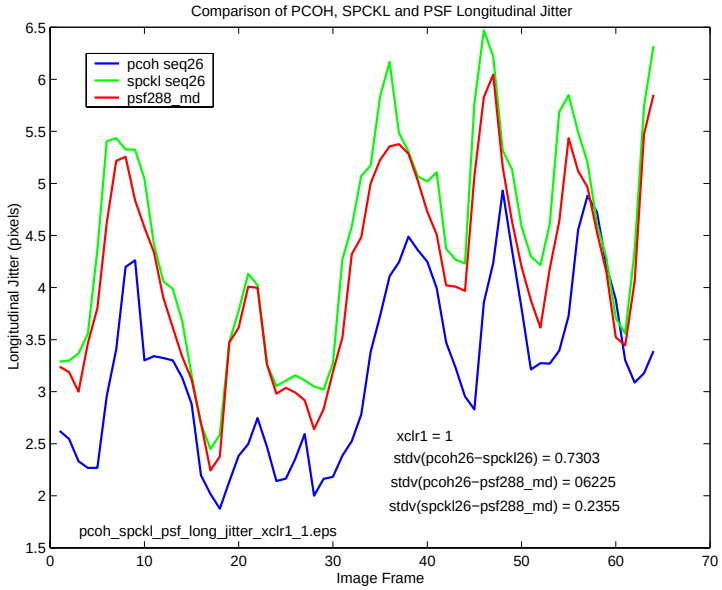

Figure 20. Comparison of PCOH, SPCKL and PSF Longitudinal Jitter.

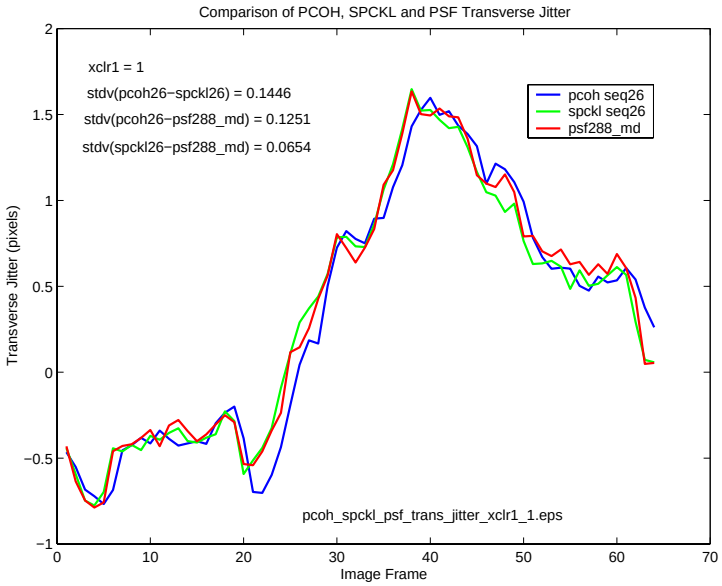

Figure 21. Comparison of PCOH, SPCKL and PSF Transverse Jitter.